


Coherence resonance in neuronal populations: Mean-field versus network modelEmre Baspinar^{1,*}, Leonhard Schülen^{2,†}, Simona Olmi^{1,3,4,‡} and Anna Zakharova^{2,4,§}¹*Inria Sophia Antipolis Méditerranée Research Centre, 2004 Route des Lucioles, 06902 Valbonne, France*²*Institut für Theoretische Physik, Technische Universität Berlin, Hardenbergstraße 36, 10623 Berlin, Germany*³*CNR - Consiglio Nazionale delle Ricerche - Istituto dei Sistemi complessi, 50019, Sesto Fiorentino, Italy*⁴*Joint Senior Authorship* (Received 18 September 2020; revised 22 January 2021; accepted 22 February 2021; published 15 March 2021)

The counterintuitive phenomenon of coherence resonance describes a nonmonotonic behavior of the regularity of noise-induced oscillations in the excitable regime, leading to an optimal response in terms of regularity of the excited oscillations for an intermediate noise intensity. We study this phenomenon in populations of FitzHugh-Nagumo (FHN) neurons with different coupling architectures. For networks of FHN systems in an excitable regime, coherence resonance has been previously analyzed numerically. Here we focus on an analytical approach studying the mean-field limits of the globally and locally coupled populations. The mean-field limit refers to an averaged behavior of a complex network as the number of elements goes to infinity. We apply the mean-field approach to the globally coupled FHN network. Further, we derive a mean-field limit approximating the locally coupled FHN network with low noise intensities. We study the effects of the coupling strength and noise intensity on coherence resonance for both the network and the mean-field models. We compare the results of the mean-field and network frameworks and find good agreement in the globally coupled case, where the correspondence between the two approaches is sufficiently good to capture the emergence of coherence resonance, as well as of anticoherence resonance.

DOI: [10.1103/PhysRevE.103.032308](https://doi.org/10.1103/PhysRevE.103.032308)**I. INTRODUCTION**

All real-world processes are affected by random fluctuations that are intrinsically produced by the system itself and/or introduced by the extrinsic mechanisms to the system. The fluctuations are modeled mathematically as noise [1–3]. In neural networks, noise occurs naturally, for example, due to random synaptic input from other neurons, spontaneous neural activity, or random opening and closing of ionic channels resulting in so-called intrinsic brain noise [4–6]. Investigation of noise impact in the brain, and in nonlinear dynamical networks in general, is a challenging problem. Noise can give rise to peculiar dynamic behavior, e.g., stochastic bifurcations [2,7,8] or stochastic synchronization [9,10]. It can even induce partial synchronization patterns such as chimera states [11–15]. Intriguingly, random fluctuations do not always have a destructive impact deteriorating the regularity of a deterministic system. Instead they can play a constructive role and lead to an increase of coherence for increasing noise intensities. The most prominent examples are stochastic resonance [16–29] that is observed for periodically driven bistable systems and *coherence resonance* that takes place in autonomous systems, i.e., under purely noise excitation without any periodic driving signal [7,30–43].

The counterintuitive phenomenon of coherence resonance was originally detected for an excitable FitzHugh-Nagumo (FHN) neuron [31]. It describes a nonmonotonic behavior of the regularity of noise-induced oscillations in the excitable regime, leading to an optimal response in terms of regularity of the excited oscillations for an intermediate noise intensity. Since the discovery of coherence resonance, it has been investigated theoretically and experimentally in various systems and networks [11,13,38,43–50]. It has been shown that coherence resonance can be observed not only in excitable [31,51] but also in nonexcitable systems [7,8,10,40–42]. Depending on the nature of the external noisy inputs, different mechanisms for coherence resonance have been observed, like the double coherence resonance, occurring for an optimal combination of noise variance and correlation of inputs stimulating a single FHN neuron [52,53]. On the other hand, in complex networks of FHN units, the existence of coherence resonance has been reported for one-layer [50] and two-layer [54] networks. Further topologies include local, nonlocal, global coupling, and lattice networks as well as more complex structures such as random or small-world networks [50,55–59].

Interestingly, large ensembles of neurons in the brain demonstrate a rich variety of coherent dynamics at the macroscopic scale which results from random perturbations [60]. Therefore, understanding coherence resonance is important for the study of brain and neural networks. Coherence is significant for communication between brain regions [61] and, as recently suggested in Ref. [62], the improvement of neural communication can be reached via coherence resonance. In

*emre.baspinar@inria.fr

†l.schuelen@campus.tu-berlin.de

‡simona.olmi@fi.isc.cnr.it

§anna.zakharova@tu-berlin.de

more detail, the brain adjusts its internal noise to maximize the coherence. Furthermore, information processing and its encoding for transmission to different areas of the brain require a coherent activity of neuronal populations. In particular, information processing in the brain can be represented as a nonstationary spatiotemporal process of activity propagation [63,64]. In this view, brain activity during task conditions simultaneously evolves in a hierarchy of characteristic network activations. For instance, information processing in sensorimotor coordination [65] and auditory, visual, and linguistic tasks [66] show robust propagation through well-tuned activation chains of characteristic subnetworks. Especially in the sensory cortex, many neurons locally sensitive to similar stimulus features give a similar response to a given input stimulus (see, for example, Refs. [67–69] for neurophysiological studies, and also Refs. [70–73] for some models using the local tuning feature of neurons). This suggests that the activity of such neurons can be measured and studied at a macroscopic scale, which provides reliable data due to the averaging effects diminishing the independent chaotic random behaviors of single neurons observed at a microscopic scale.

The growing interest in the phenomenon of coherence resonance for neural networks is confirmed by a number of works [50,55–58,74,75], including very recent ones [54,59,62]. While the majority of these investigations is based on numerical simulations or on experimental data, much less attention is paid to the analytical treatment of coherence resonance in complex networks. Although analytical treatment has been provided for single systems (e.g., for the FHN system in Ref. [76], for the generalized van der Pol oscillator in Ref. [10], and for the leaky integrate-and-fire neuron in Ref. [77]), it remains a demanding problem for networks. Here we address this challenging question by developing a mean-field framework for analyzing coherence resonance in neural populations. Using a paradigmatic model of FHN neurons, we study the phenomenon of coherence resonance both at the network level (i.e., where we model each neuron in the population as a perturbed coupled FHN system) and in the *mean-field limit* (known also as *thermodynamic limit*), which is the asymptotic limit of a state variable quantity representing the averaged network behavior in the infinite size limit.

Our main contributions are at both theoretical and numerical levels. At the theoretical level, we attempt to provide a mathematical understanding of the results obtained from numerical simulations of locally and globally coupled neural networks presented in Ref. [50]. Classical mean-field approach requires a network where the coupling is dense within. In other words, the coupling must be scalable with the total number of neurons in the network. Network topologies with one-dimensional coupling, like chains and rings, express coherence patterns such as chimera states [78] and coherence resonance [50]. One may ask if the intricate mechanisms of coherence patterns in networks with aforementioned coupling can be grasped via a mean-field approach. In general, the classical mean-field approach is not applicable to one-dimensional coupling where the coupling remains local and not dense in the network. Nevertheless, it is possible to use an approximate definition of the mean-field system and take advantage of coupling symmetries. In certain cases, this will allow us to provide a first approximation of the

mean-field limit of a locally coupled network, which coincides with the network framework for small noise intensities and low excitability threshold. For the globally coupled case, we employ the mean-field description provided in Refs. [79,80] for a generic family of stochastic differential equations of the stochastic FHN type and we decline the model in two versions, which differ from the number of employed noise terms: a single additive noise term in the differential equation for the recovery variable or two different noise terms, one for each variable equation. The latter mean-field model, which represents an extended version of the former, has been designed to take into account both the noise effect arising from the small random changes occurring in the coupling media and the noise effect experienced due to the random switching of the ionic channels when arranging the passive flow of the ionic current through the pores between neurons: this flow, together with the charge carriers, has a stochastic nature [81–83]. In similar frameworks, it has been considered either the intrinsic noise modeling the channel gate random switching or the external noise modeling the small random changes observed in the coupling current. Inclusion of both noise sources simultaneously has been restricted to the theory of stochastic differential equations [84,85] only. Here we provide an attempt to study the coherent behavior induced by combined effects of two noise sources in a globally coupled framework, both at network and at mean-field level.

At the numerical level, we investigate the emergence of antcoherence resonance in the globally coupled framework, which results in different outcomes depending on the investigated model. When one single noise term is present, antcoherence resonance does not emerge in the system, while, when two noise terms are present, antcoherence resonance emerges for large noise intensity and it is characterized by an alteration of the dynamics, which is now guided by the noise.

The paper is organized as follows. In Sec. II, we provide the network settings for each topological architecture. Afterward, we explain the associated mean-field frameworks in Sec. III. In Sec. IV, we explain the experimental setting and present our simulation results where we compare the coherence resonance results obtained from the mean-field systems and network framework to find out to which level they provide the same outcome, i.e., we identify the limitations of the mean-field approach. Finally, we give the conclusions in Sec. V.

II. NETWORK EQUATION

Several dynamical models have been proposed to study both single neuron and coupled neuronal population behaviors, such as the Hodgkin-Huxley model [86], or other conductance-based models, like the Morris-Lecar model [87]. Conductance-based models are the simplest possible biophysical representation of an excitable cell, such as a neuron, in which its protein molecule ion channels are represented by conductances and its lipid bilayer by a capacitor. However, other types of models have been developed that predict the dynamics of the membrane output voltage as a function of electrical stimulation at the input stage, like Hindmarsh and Rose [88], integrate-and-fire [89–91], or the Galves-Löcherbach model [92]. At the mean-field level, heuristic firing rate models are commonly used, like the Wilson-Cowan

excitatory-inhibitory neural mass model [93,94] and its stochastically modified versions [95]. Only recently have neural mass models been developed that are not derived heuristically but that reproduce exactly the dynamics of excitatory and inhibitory networks of spiking neurons for any degree of synchronization [96–99]. In particular, these neural masses reproduce the macroscopic dynamics of quadratic integrate-and-fire neurons, which are normal forms for the saddle node on a limit cycle bifurcation (SNIC) [100] and describe, in general, the dynamics of class I neurons (i.e., neurons with a continuous gain function), to which belong the Hindmarsh-Rose model and the Morris-Lecar model under some circumstances. In the present paper, we are particularly interested in the celebrated FHN model [101,102], which represents a reduced version of the Hodgkin-Huxley model. It still captures closely the dynamical behaviors produced by the Hodgkin-Huxley model and has the advantage of facilitating efficient large-scale simulation of groups of neurons.

Network equations describe the dynamics of each neuron belonging to the network at a microscopic level. The classical deterministic FHN equations describing the evolution of a single neuron belonging to a coupled population read as

$$\begin{aligned} \varepsilon \frac{du_i(t)}{dt} &= f(u_i(t), v_i(t)) + \frac{\sigma}{2P} \sum_{j=i-P}^{i+P} [u_j(t) - u_i(t)] \\ &= u_i(t) - \frac{u_i(t)^3}{3} - v_i(t) + \frac{\sigma}{2P} \sum_{j=i-P}^{i+P} [u_j(t) - u_i(t)], \\ \frac{dv_i(t)}{dt} &= g_a(u_i(t)) = u_i(t) + a, \end{aligned} \quad (1)$$

where σ is a positive constant denoting the coupling strength. u_i and v_i represent the activator (membrane potential) and inhibitor (recovery) variables of the i th neuron, respectively ($i = 1, \dots, N$, where N is the population size). $\varepsilon > 0$ is responsible for the timescale separation of fast activator and slow inhibitor, being a small parameter. Here, we fix $\varepsilon = 0.01$. Parameter a determines the nature of the equilibrium points and thus the excitability threshold of the isolated, uncoupled neuron. In particular, the parameter a serves as a threshold in our model and determines whether the single neuron is in the excitable $|a| > 1$ or in the oscillatory $|a| < 1$ regime. The single neuron undergoes a Hopf bifurcation when $a = 1$. Finally P denotes, for the i th neuron, the number of its nearest neighbors in each direction of the ring. Thus, it determines the topology of the population: if $P = 1$, we have local coupling, if $P = (N - 1)/2$ (we assume N is odd), we have global coupling and, finally, if $1 < P < (N - 1)/2$, we have nonlocal coupling.

We assign a stochastic behavior to the system by adding a Gaussian white noise term $dW_i(t)$ to the recovery variable equation of each neuron, as described in Refs. [50,54]. The noise term $dW_i(t)$ is built, for each neuron i , from an independent Wiener process. More precisely,

$$\mathbb{E}[dW_i(t)] = 0, \quad \mathbb{E}[dW_i(t)dW_j(t')] = \delta((i-j)(t-t')), \quad \forall i, j, \quad (2)$$

with \mathbb{E} and δ denoting expectation value and Dirac delta function, respectively. For the sake of simplicity, we drop showing

the time dependency explicitly from now on, as long as the otherwise is required. The stochastic FHN equations read as follows:

$$\begin{aligned} \varepsilon du_i(t) &= f(u_i(t), v_i(t))dt + \frac{\sigma}{2P} \sum_{j=i-P}^{i+P} [u_j(t) - u_i(t)]dt, \\ dv_i(t) &= g_a(u_i(t))dt + \sqrt{2D} dW_i(t), \quad i = 1, \dots, N, \end{aligned} \quad (3)$$

where D denotes the level of noise intensity. Gaussian white noise is intended to represent triggering perturbations that alters the state of the system. Here we focus on the dynamics of neuronal populations in their excitable regime. In this regime, a sufficiently strong perturbation triggers the whole population to produce spikes before the population comes back to its steady state. If the perturbation is not strong enough, the population relaxes back to its unique stable steady state without producing a spike. In particular, we are interested in the state of the network characterized by the best temporal regularity of the noise-induced spiking dynamics achieved for an intermediate optimal noise intensity, i.e., when the network undergoes coherence resonance. In Sec. IV, when comparing the network dynamics emergent in the network with the mean-field prediction, in the globally coupled regime, we will also integrate a second set of equations that differ from Eqs. (3) by adding a second noise term $\sqrt{2\varepsilon\bar{D}} d\bar{W}_i(t)$ in the first differential equation, where \bar{D} denotes the level of noise intensity and $d\bar{W}_i(t)$ represents, as before, a Gaussian noise source. The reason for this will become clear when introducing the extended version of the mean-field limit associated to the globally coupled FHN system [see Eqs. (9) in Sec. III].

A. Macroscopic indicators of coherence resonance

Coherence resonance characterizes the emergence of relatively coherent noise-induced oscillations occurring for an optimal noise intensity. It was initially found in a single FHN system in the excitable regime and later detected for neural networks. There exist several different measures for quantifying coherence resonance, such as the normalized standard deviation of the interspike interval (ISI), the correlation time, and the signal-to-noise-ratio [30,31,41]. Since in the present paper we deal with a neural model showing spiking behavior, it is convenient to use the standard deviation of the ISI, defined as

$$R_{\text{ISI}} = \frac{\sqrt{\langle t_{\text{ISI}}^2 \rangle - \langle t_{\text{ISI}} \rangle^2}}{\langle t_{\text{ISI}} \rangle}, \quad (4)$$

where t_{ISI} is the time between two subsequent spikes and $\langle \dots \rangle$ indicates the average over the time series. As the FHN system does not have a hard threshold, we identify artificially a spike as emitted in the network whenever a unit crosses the value $u = 0$ from below. That way, we ignore all subthreshold oscillations. A system undergoing coherence resonance will show a pronounced minimum in the value of R_{ISI} [31]. The definition (4) is limited to characterizing coherence resonance for a single FHN oscillator. For a network of oscillators, coherence resonance can be measured by redefining R as follows

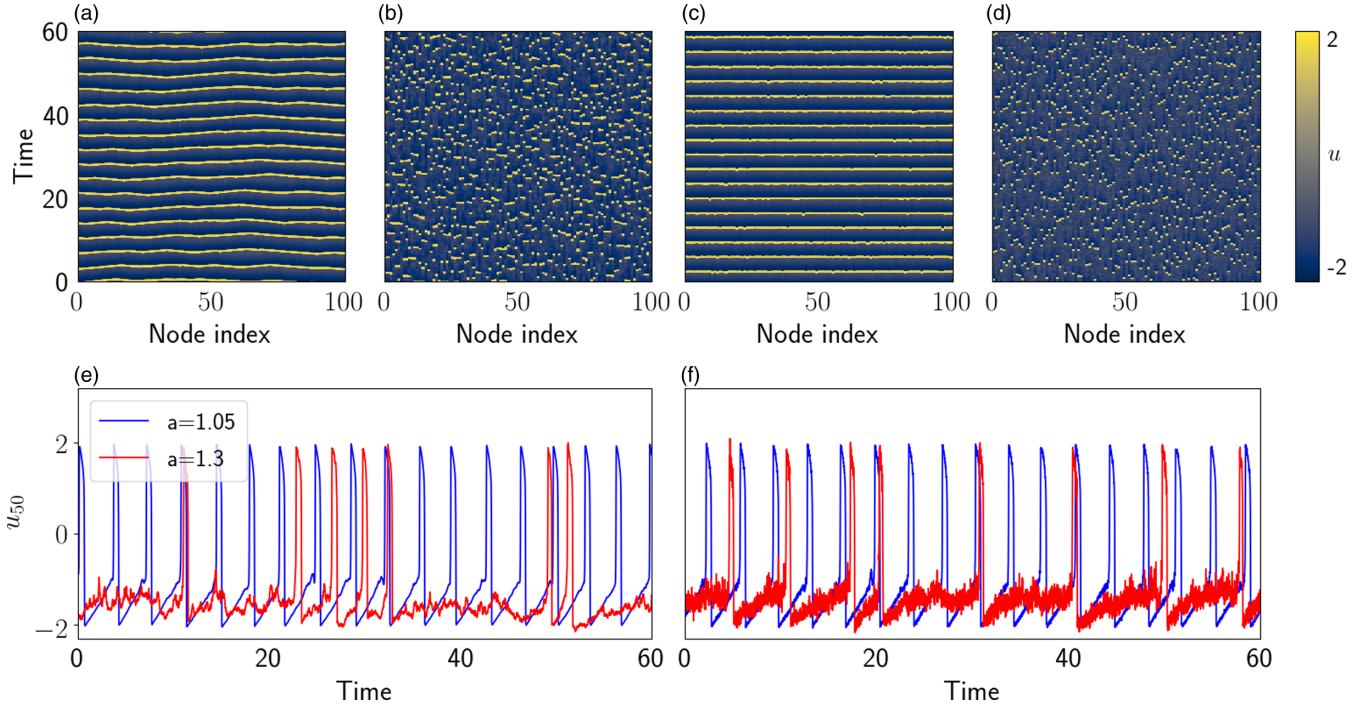


FIG. 1. Space-time plots for optimal D values (i.e., R takes minimum values) for different network topology and a values: (a) a locally coupled network with $a = 1.05$ and $D = 0.001$, (b) a locally coupled network with $a = 1.3$ and $D = 0.08$, (c) a globally coupled network with $a = 1.05$ and $D = 0.0008$, (d) a globally coupled network with $a = 1.3$ and $D = 0.0158$. Time series of one selected neuron in a locally (e) and globally (f) coupled network for $a = 1.05$ (blue) and $a = 1.3$ (red). Other parameters: $N = 100$, $\varepsilon = 0.01$, $\sigma = 0.1$.

[50]:

$$R = \frac{\sqrt{\langle \overline{t_{\text{ISI}}^2} \rangle - \langle \overline{t_{\text{ISI}}} \rangle^2}}{\langle \overline{t_{\text{ISI}}} \rangle}, \quad (5)$$

where the overbar indicates the additional average over nodes.

To illustrate the dynamics of the system in the regime of coherence resonance, we provide here space-time plots and time series for a locally and globally coupled network in the stochastic regime (see Fig. 1). In more detail, we show the dynamical behavior emerging for different threshold parameter values ($a = 1.05$ and $a = 1.3$) for the locally coupled [Figs. 1(a) and 1(b)] and the globally coupled [Figs. 1(c) and 1(d)] cases. In the locally coupled case we observe, for the lower threshold value ($a = 1.05$), coherent response among all network elements that spike regularly and nearly at the same time (panel a), resulting in a very low value of $R = 0.056$. The case of higher threshold $a = 1.3$ shows a more irregular response, while still having a rather small value of $R = 0.518$ [Fig. 1(b)]. When the threshold is increased, it is harder for the system to overcome it. A similar scenario emerges when passing from local to global coupling. For the lower threshold value, the coherent response of the network is clearly observable. In this case, the FHN neurons spike in a highly synchronized way [see the straight yellow lines in Fig. 1(c)] due to the fact that each element receives the input from the entire network being connected with all the others. The simultaneous interaction among all neurons enhance them to overcome the threshold all at once. At the contrary, in the locally coupled case, each neuron pulls only its immediate neighbors over the threshold, which explains why the

excitation needs some time to travel over the ring. Similarly to what shown in Fig. 1(b), the case of higher threshold value gives a more irregular picture even in the globally coupled configuration [Fig. 1(d)]. The same conclusions can be drawn looking at the time series of single units. In particular, in Fig. 1(e), the time series of one selected neuron in the locally coupled network for $a = 1.05$ (blue curve) and $a = 1.3$ (red curve) are shown, while Fig. 1(f) illustrates the time series of the same element in the globally coupled case for $a = 1.05$ (blue curve) and $a = 1.3$ (red curve). The higher temporal regularity for the lower threshold parameter a can be clearly seen for both coupling topologies.

III. MEAN-FIELD POPULATION EQUATIONS

A. Globally coupled equations

In the globally coupled mean-field framework, we have $P = N/2$ as $N \rightarrow \infty$. We assume that the coupling strength is the same and constant for all neurons in a single population. To avoid using negative indices in Eqs. (3) we change the indexing of the coupling term according to

$$\sum_{j=1}^{N+1} [u_i - u_j], \quad (6)$$

without losing the generality.

We emphasize that the noise terms in Eqs. (3) are assumed to be independent and identically distributed for each neuron and also for each state variable. This allows us to describe, in the thermodynamic limit, each state variable of a neuron as a continuous set of random variables, each one corresponding

to an instant of time. In other words, each state variable can be thought of as a stochastic process representing the values of the state variable changing randomly in time. As such, the state variables u_i and v_i of the i th neuron (for any $i = 1 \dots, N$) evolve in accordance with their associated probability distributions, which converge in the thermodynamic limit, to the ones of the mean-field state variables u and v characterized by

$$\lim_{N \rightarrow \infty} \max_{i=1, \dots, N} \mathbb{E}[\sup_{s \leq t} (u_i(s) - u(s))^2] = 0,$$

$$\lim_{N \rightarrow \infty} \max_{i=1, \dots, N} \mathbb{E}[\sup_{s \leq t} (v_i(s) - v(s))^2] = 0. \quad (7)$$

As shown in Refs. [79,80], the state variables u and v comprise the solution to the following mean-field system:

$$\varepsilon du = f(u, v)dt + \sigma(\mathbb{E}[u] - u)dt,$$

$$dv = g_a(u)dt + \sqrt{2D}dW, \quad (8)$$

where dW denotes Gaussian white noise with the properties given in Eqs. (2) and D defines the noise intensity level. Here σ represents the coupling constant, as introduced in the network Eqs. (3). This mean-field equation was derived in Refs. [79,80] from a network of FHN neurons of the same type as Eqs. (3), based on two steps: (i) the first step shows that a unique solution to Eqs. (8) exists for a finite time, under the assumption that the terms f and g_a are locally sufficiently regular (locally Lipschitz); and (ii) the second step shows that for each neuron in the network, the probability distributions of the processes u_i and v_i converge toward the probability distributions of the mean-field state variables u and v , respectively.

While the mean-field framework shown in Eqs. (8) corresponds to the classical mean-field limit of the globally coupled networks of FHN oscillators of the type given in Refs. [50,54], we consider in the following an extended version of the mean-field limit associated to the globally coupled FHN system. In Refs. [79,80], it was shown that the same results and properties as in Eqs. (8) hold also for the extended version, which is adapted from Refs. [79,80], as follows:

$$\varepsilon du = f(u, v)dt + \sigma(\mathbb{E}[u] - u)dt + \sqrt{2\varepsilon\bar{D}}d\bar{W},$$

$$dv = g_a(u)dt + \sqrt{2D}dW, \quad (9)$$

where $d\bar{W}$, dW are the noise terms generated independently from a Gaussian distribution with zero mean and unit variance. We denote the noise intensity levels as \bar{D} , D . To guarantee that $d\bar{W}$ does not dominate dW , neither the whole system behavior, we impose \bar{D} to be of the same order as D . Moreover, we add the scaling term $\sqrt{\varepsilon}$, thus keeping the noise small.¹ As for Eqs. (8), the presence of $\sigma(\mathbb{E}[u] - u)dt$ requires studying the state variable u , whose solution depends on its own expectation value.

The choice of this extended model is motivated by the presence of the global coupling term: The noise effects arising from the coupling can be modeled by introducing an

additional white noise term ($d\bar{W}$) in Eqs. (8), as shown in Eqs. (9). More specifically, the additional noise on the first line of Eqs. (9) models the stochastic nature of the gap junction media, which creates small random changes in the coupling current, while the noise term in the second line models the stochastic nature of the ionic channels, i.e., the random switching of channel gates arranging the ionic current [81–83]. Finally, we remark that, when comparing the results obtained from the simulation of Eqs. (9) with those obtained from the network, the corresponding network equations are described, for consistency, by Eqs. (3) with an additional noise term, $\sqrt{2\varepsilon\bar{D}}d\bar{W}_i(t)$, in the first equation, where \bar{D} denotes the level of noise intensity for the Gaussian white noise $d\bar{W}_i(t)$.

The mean-field limit models the population behavior by employing a single FHN system once the number of the neurons in the population is sufficiently high, whereas, for the network equations, we need a separate FHN equations system for each neuron in the population. In other words, the network equations require a high-dimensional dynamical system while the mean-field limit requires only a two-dimensional dynamical system, being a good representative of the averaged dynamics of the population and making analytical treatment of the system feasible. However, studying the statistics of such a system is not trivial since the right-hand side requires the expectation of the solution of the equation. Yet, it is possible to use a semianalytical approach, where we obtain the first-moment statistics of u from numerical simulations of the network equations given by Eqs. (3), as shown in Ref. [79]. Practically, the expectation value of u will be introduced numerically in the differential Eqs. (9), by obtaining the statistics of the state variables from the network simulations. In this way, it will be possible to investigate the interplay of coupling and noise to determine the emergence of coherence resonance and to provide an analytical framework for the numerical results.

Finally, we note that, although the notation for the mean-field state variables are denoted in the same way, by u and v , for both globally and locally coupled settings, the corresponding definitions are different and, in the rest of the paper, it should be tacitly understood from the coupling type.

B. Locally coupled equations

In the locally coupled topology, $P = 1$ and the network equations for the i th neuron can be written as

$$\varepsilon du_i = f(u_i, v_i)dt + \frac{\sigma}{2}(u_{i-1} + u_{i+1} - 2u_i)dt,$$

$$dv_i = g_a(u_i)dt + \sqrt{2D}dW_i, \quad i = 1, \dots, N. \quad (10)$$

We assume to have periodic boundary conditions: the i th neuron is coupled to the $(i - 1)$ th and $(i + 1)$ th neurons for all $i \in \{1, 2, \dots, N\}$, while it holds that

$$u_{N+K} = u_K \quad \text{for all } K \in \{-N, -N + 1, \dots, N - 1, N\}. \quad (11)$$

¹The scaling with $\sqrt{\varepsilon}$ is required since u and v evolve with different time constants reflected in ε : the scaling term tunes the noise term $d\bar{W}$ in accordance with this difference while compensating the unit inconsistency arising from the diffusive character of the noise.

The average dynamics of a locally coupled system in the thermodynamic limit can be found by considering that

$$\begin{aligned} \frac{\varepsilon}{N} \sum_{i=1}^N du_i &= \frac{1}{N} \sum_{i=1}^N f(u_i, v_i) dt + \frac{\sigma}{2N} \sum_{i=1}^N (u_{i-1} + u_{i+1} - 2u_i) dt, \\ \frac{1}{N} \sum_{i=1}^N dv_i &= \frac{1}{N} \sum_{i=1}^N g_a(u_i) dt + \frac{1}{N} \sum_{i=1}^N \sqrt{2D} dW_i, \end{aligned} \quad (12)$$

where the term proportional to the coupling constant σ on the right-hand side of the first equation vanishes for $N \rightarrow \infty$. Moreover, we define in the following

$$u := \frac{1}{N} \sum_{i=1}^N u_i, \quad v := \frac{1}{N} \sum_{i=1}^N v_i, \quad (13)$$

and

$$\frac{1}{N} \sum_{i=1}^N dW_i = dW, \quad (14)$$

where dW is a Gaussian white noise as a result of the central limit theorem. We emphasize that the definitions of mean-field variables in (13) are different from the globally coupled case. A different definition is required since the classical mean-field formalism is not applicable here, where the coupling is not dense, i.e., not scalable to $1/N$.

It is not straightforward to write the average dynamics directly from Eqs. (12) (neither the exact mean-field limit) due to the nonlinearity of f . To handle the nonlinearity, we approximate the state variables u_i as random variables distributed according to a Gaussian distribution, as described in Ref. [103] (see also Refs. [104–107] for details regarding the use of Gaussian random variables in such approximations). This approximation assumes that the excitable system is sufficiently close to the equilibrium point and the noise intensity D is small. We employ the law of large numbers (see, for example, Ref. [108]), more precisely

$$\frac{1}{N} \sum_{i=1}^N u_i = \mathbb{E}[u_i] \quad \text{as } N \rightarrow \infty, \quad (15)$$

and write the mean-field limit from the average dynamics given in Eqs. (12). Since we approximate u_i as a Gaussian random variable with expectation value u and variance ρ^2 , we have

$$\begin{aligned} \mathbb{E}[u_i] &= \frac{1}{\sqrt{2\pi\rho^2}} \int_{-\infty}^{\infty} u_i e^{-\frac{(u_i-u)^2}{2\rho^2}} du_i = u, \\ \mathbb{E}[u_i^3] &= \frac{1}{\sqrt{2\pi\rho^2}} \int_{-\infty}^{\infty} u_i^3 e^{-\frac{(u_i-u)^2}{2\rho^2}} du_i = u^3 + 3\rho^2 u. \end{aligned} \quad (16)$$

By implementing Eqs. (14)–(16) in Eqs. (12) we find, in the limit $N \rightarrow \infty$, that

$$\varepsilon du = f(u, v) dt - \rho^2 u dt, \quad dv = g_a(u) + \sqrt{2D} dW, \quad (17)$$

and more explicitly

$$\begin{aligned} \varepsilon du &= \left((1 - \rho^2)u - \frac{u^3}{3} - v \right) dt, \\ dv &= (u + a) dt + \sqrt{2D} dW. \end{aligned} \quad (18)$$

The fact that the coupling term vanishes in Eqs. (12) indicates that there is no effect of the coupling at the mean-field level. Moreover, since we do not have any information about ρ a priori in the mean-field framework, we obtain the ρ values from the numerical network simulations and introduce them at each time sample when we perform the numerical integration of Eqs. (18).

The mean-field variables are here approximated as random variables distributed according to a Gaussian distribution and they represent the mean value of the network variables. Therefore, in the locally coupled case, we propose a mean-field model which represents an approximation of the averaged network. Indeed, the proposed mean-field model (18) for the locally coupled framework will prove successful only in a subset of the whole parameter set. At the contrary, in the globally coupled framework, the approach proposed in Refs. [79,80] does not require any approximation and provides a precise description of the mean-field variables. In particular, it provides a set of mean-field variables with the same probability distribution as the network variables calculated in the infinite size limit. Therefore, the mean-field variables share the same statistics (e.g., mean value, standard deviation of the ISIs) as the network in the limit of infinite numbers of neurons, although they are not necessarily equal to the average of the network variables.

C. Nonlocally coupled equations

Finally, we consider the intermediate nonlocally coupled case with $1 < P < \frac{N}{2}$. It is convenient to distinguish between two cases that represent two classes of systems [109]: sparse (or strongly diluted) networks, where $P \ll N$, and specifically P is independent of N as $N \rightarrow \infty$; massive networks, where P is proportional to the network size N . In our ring topology, these cases can be translated in the following limits:

$$\lim_{N \rightarrow \infty} \frac{P}{N} = 0 \quad \text{and} \quad \lim_{N \rightarrow \infty} \frac{P}{N} = C, \quad (19)$$

where C is a constant value and $C \leq 1/2$ for the definition of ring topology. In the first case ($P \ll N$), if we fix P to be a constant connectivity, we can write the following averaged network equations for $N \rightarrow \infty$:

$$\begin{aligned} \frac{\varepsilon}{N} \sum_{i=1}^N du_i &= \frac{1}{N} \sum_{i=1}^N f(u_i, v_i) dt + \frac{1}{N} \sum_{i=1}^N \frac{\sigma}{2P} \\ &\quad \times (u_{i-P} + \dots + u_{i+P} - 2(P+1)u_i) dt, \\ \frac{1}{N} \sum_{i=1}^N dv_i &= \frac{1}{N} \sum_{i=1}^N g_a(u_i) dt + \frac{1}{N} \sum_{i=1}^N \sqrt{2D} dW_i, \end{aligned} \quad (20)$$

which turns out to be the same as the locally coupled system given in Eqs. (18). In the second case ($P \propto N$), we may write P as a function of N , i.e. $P = P(N)$, such that the same limit holds for P and N , when $N \rightarrow \infty$. This means that, starting from the mean-field system presented for the globally coupled case in Eqs. (8), it should be possible to straightforwardly derive a set of equations for the particular case $P = P(N)$, as long as the coupling constant σ is rescaled in accordance with the limit value comparable to C .

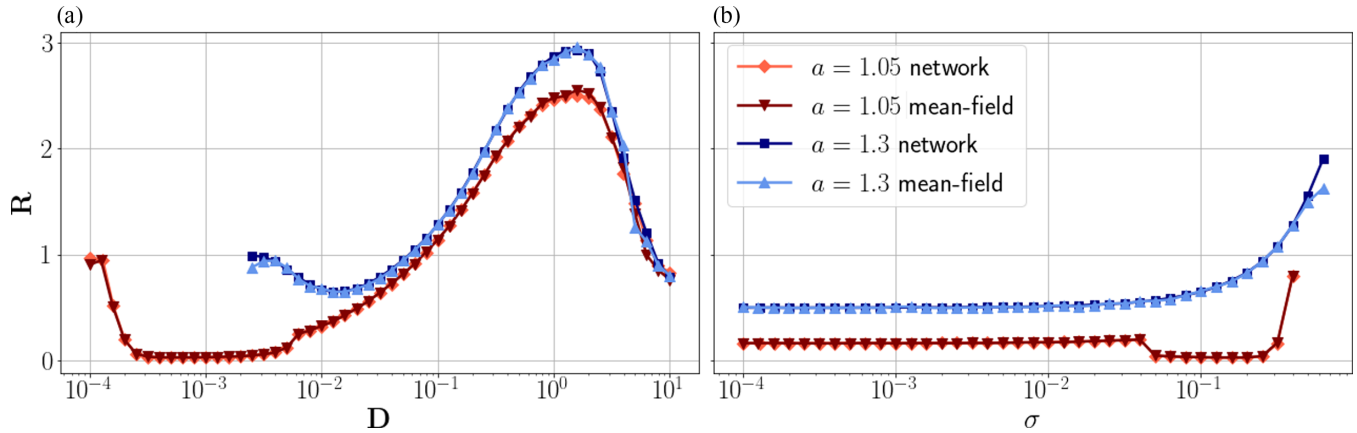


FIG. 2. Normalized standard deviation of the interspike interval R for a globally coupled network with noise terms in both system variable equations and its mean-field system: (a) for fixed coupling strength $\sigma = 0.1$ and varying noise intensity D ; (b) for fixed noise intensity ($D = 0.001$ for $a = 1.05$ and $D = 0.012$ for $a = 1.3$) and varying coupling strength σ . In both panels, light red diamonds identify the network while dark red downward triangles identify the mean-field results for $a = 1.05$; dark blue squares identify the network while light blue upward triangle identify the mean-field simulations for $a = 1.3$. The results are obtained by integrating over 10 000 time units and then averaging over time, oscillators, and realizations (five simulations for each σ). The x axis has logarithmic scaling. Other parameters: $N = 100$, $\varepsilon = 0.01$.

We conclude that nonlocally coupled topology cannot be treated as a separate one, since its dynamics can be attributable to the one emergent in either sparse or massive networks. This case confirms what already found in the literature: (i) for massive networks, i.e., when the connectivity scales with N , the network behaves like a globally coupled system with a rescaled coupling constant to account for the different fraction of active links [110]; and (ii) for sparse networks, characterized by constant connectivity, not increasing with N , the thermodynamic limit shows a completely different behavior, typical of locally coupled topology [111].

IV. SIMULATION RESULTS

A. Globally coupled framework

Here we study the role of noise intensity D and coupling strength σ in inducing coherence resonance in a network of globally coupled FHN oscillators. In particular, for the mean-field model we initially simulate the system given by Eqs. (9), by employing the classical Euler-Maruyama numerical scheme, as detailed in Appendix A. We measure R in two different parameter settings: First, we increase D , keeping all parameters fixed and, second, we increase σ , keeping all the other parameters fixed. The results are shown in Fig. 2 for different excitability threshold values. Note that the x axis is logarithmic in both cases.

Coherence resonance is visible both for $a = 1.05$ and for $a = 1.3$ [Fig. 2(a)], where a minimum in R emerges; the location of the minimum depends on the excitability threshold value and it occurs for different noise intensities D in the two cases. It is worth noticing here that, if the system is closer to the Hopf bifurcation point, i.e., for $a = 1.05$, it requires lower noise intensity for coherence resonance to occur. On the other hand, if the system is further away from the Hopf bifurcation point, i.e., for $a = 1.3$, the system requires higher noise intensity. An interesting observation is that for both $a = 1.05$ and $a = 1.3$, the $R(D)$ -curve has both minimum and maximum

[Fig. 2(a)]. The occurrence of the maximum is associated with the phenomenon of antcoherence resonance investigated in Refs. [112–114]. Here we show that the antcoherence is captured by the mean-field analysis.

To study the effects of coupling strength on the above observed coherence resonance, we measure R as σ is varied, for fixed D , in two different parameter settings: First, for $a = 1.05$ where we fix $D = 0.001$ and, second, for $a = 1.3$ with $D = 0.012$ [Fig. 2(b)]. We observe for the case $a = 1.05$ that coherence resonance is enhanced for a certain range of coupling strength (when $0.05 \leq \sigma < 0.25$). Several other works have also shown that coherence resonance can be enhanced by choosing appropriate coupling strengths [44,49,56]. Here we demonstrate that this feature can be captured well in the mean-field framework. For the higher value of excitability threshold, i.e., $a = 1.3$, the same can be observed. As can be seen in Fig. 2(b), the network behavior is captured well in the mean-field framework.

The emergence of antcoherence resonance is due to the increasing role played by the noise, which destroys the refractory time proper of each neuron, thus allowing for infinitely small ISIs. This can be seen by plotting the probability distribution $p(t_{ISI})$ of the time between two successive spikes t_{ISI} , for increasing noise intensity (see Figs. 3 and 4 for $a = 1.05$ and $a = 1.3$, respectively). In particular, Fig. 3 reports the probability distributions for $D = 0.001$ [Fig. 3(a)], $D = 0.03981$ [Fig. 3(b)], $D = 1.58489$ [Fig. 3(c)] and $D = 3.16228$ [Fig. 3(d)], thus characterizing four different states of the curve shown in Fig. 2(a), including the minimum and the maximum of the curve. At the minimum ($D = 0.001$), the probability distribution is very peaked: the spike emission is coherent and all neurons spike with almost the same time interval. For increasing noise intensity ($D = 0.03981$), the distribution becomes wider and longer times are possible between successive spikes. Finally, at the maximum ($D = 1.58489$) and for wider noise intensities, noise guides the dynamics and destroys the coherence: The presence of infinitely

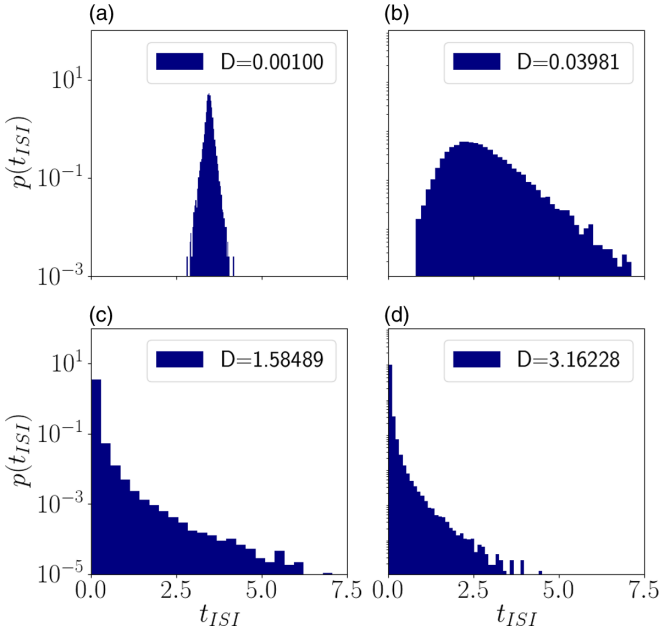


FIG. 3. Probability distribution $p(t_{ISI})$ of the measured interspike intervals t_{ISI} in a globally coupled network with $a = 1.05$ and with noise terms in both system variable equations for noise intensity (a) $D = 0.001$, (b) $D = 0.03981$, (c) $D = 1.58489$, (d) $D = 3.16228$.

small ISIs is the signature of a fluctuation-driven dynamics, where neurons overcome the threshold very often due to the high noise intensity.

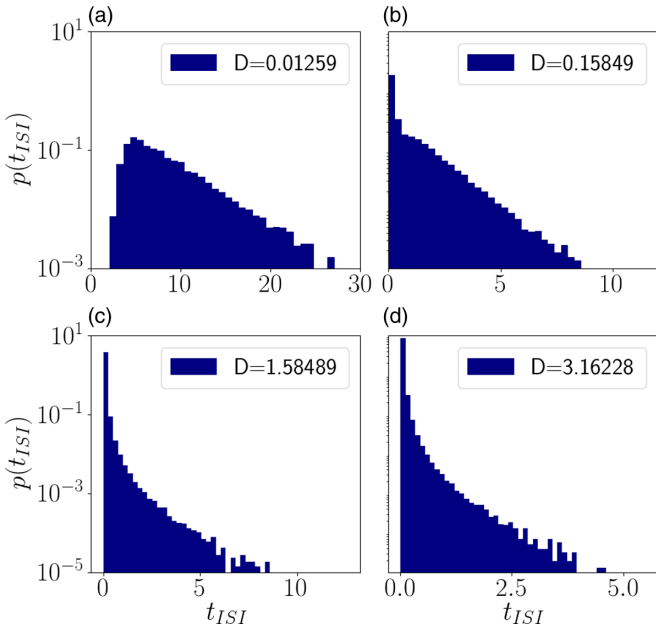


FIG. 4. Probability distributions $p(t_{ISI})$ of the measured interspike intervals t_{ISI} in a globally coupled network with $a = 1.3$ and with noise terms in both system variable equations for noise intensity (a) $D = 0.01259$, which corresponds to the minimum of the curve shown in Fig. 2(a); (b) $D = 0.15849$; (c) $D = 1.58489$ corresponding to the maximum in Fig. 2(a); (d) $D = 3.16228$.

Similar conclusions can be drawn from Fig. 4, which describes four different states of the curve previously reported in Fig. 2(a), corresponding to $D = 0.01259$ [Fig. 2(a)], $D = 0.15849$ [Fig. 2(b)], $D = 1.5849$ [Fig. 2(c)] and $D = 3.16228$ [Fig. 2(d)]. Since the system requires higher noise intensity to achieve coherence resonance at $a = 1.3$, the level of coherence is lower with respect to the previous case and the probability distribution at the minimum ($D = 0.01259$) is less peaked than the corresponding case shown in Fig. 3(a). For higher noise intensities [Figs. 2(b)–2(d)], it is possible to register t_{ISI} values that are smaller than the refractory time due to the presence of strong fluctuations that guide the network dynamics, thus triggering the antcoherence phenomenon.

The shown results are stable with respect to the integration scheme and do not depend on the chosen network size. More details are given in Appendix A for the stability of the mean-field solution with respect to the integration scheme, while the impact of network size on the results is further discussed in Appendix B. In the following, we consider the globally coupled mean-field system with only one noise term, as given in Eqs. (8), which is the exact mean-field limit in the globally coupled case of Eqs. (3). As previously done for the extended mean-field model, we study the role of noise intensity D and coupling strength σ in inducing coherence resonance and compare the results obtained from the mean-field and network simulations.

Figure 5 shows the results for $a = 1.05$ and $a = 1.3$, respectively. In both cases, coherence resonance is visible and a minimum in R emerges [Fig. 5(a)]. As for the extended mean-field model, the location of the minimum depends on the excitability threshold value and it occurs for higher noise intensities D when a higher excitability threshold is chosen. Moreover, we observe that R values obtained from the mean-field framework and the direct network simulation overlap almost completely for the whole considered range of noise values. To study the effects of coupling strength on the observed coherence resonance, we have measured R as σ is varied for fixed D [Fig. 5(d)]: For both excitability threshold values, coherence resonance can be obtained by choosing appropriate coupling strengths. Also for this numerical experiment we see good agreement between the network and the mean-field system.

Finally, we observe a different behavior, in terms of antcoherence resonance, for the cases shown in Figs. 5(a) with respect to the cases shown in Fig. 2(a): Differently from the extended model, in the latter case we do not observe the presence of a relative maximum for high noise intensity values. A maximum appears in the mean-field system, for very small values of noise intensity, similarly to what was reported in Ref. [112], where antcoherence resonance has been shown to appear for a single stochastic FHN neuron, due to the mixing of two different timescales: When adding additive noise of small intensity, the neuron responds in what appears to be trains consisting of a few number of enchainned pulses. While the pulses belonging to a single spike train are separated by a small deterministic timescale separation, the time interval between two consecutive pulses is longer and unpredictable. However, the same conjecture cannot be extended to our globally coupled network of FHN neurons since we observe, in the network system, a purely Poissonian statistics, with the

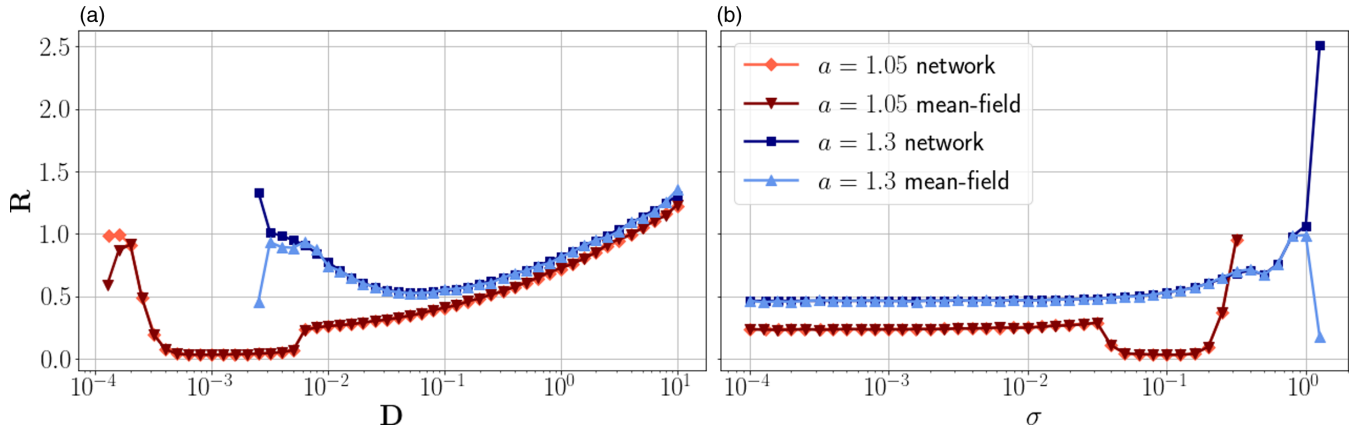


FIG. 5. Normalized standard deviation of the interspike interval R for a globally coupled network with single noise term as given in Eqs. (3) and its mean-field system (a) for fixed coupling strength $\sigma = 0.1$ and varying noise intensity D . (b) For fixed noise intensity ($D = 0.00079$ for $a = 1.05$ and $D = 0.05012$ for $a = 1.3$) and varying coupling strength σ . In both panels, light red diamonds identify the network while dark red downward triangles identify the mean-field results for $a = 1.05$; dark blue squares identify the network while light blue upward triangles identify the mean-field simulations for $a = 1.3$. The results are obtained by integrating over 10 000 time units and then averaging over time, oscillators, and realizations (for five simulations each). The x axis has logarithmic scaling. Other parameters: $N = 100$, $\varepsilon = 0.01$.

Poisson limit $R = 1$ reached from the above. Therefore, we conclude that the maximum in the mean-field system is rather an artificial effect due to the poor prediction of the model in the Poissonian regime.

B. Locally coupled framework

In the following, we show the results obtained from the investigation of the mean-field system in the locally coupled regime [Eqs. (18)], which has been simulated by applying the discrete scheme given in Eqs. (A3) and reported in Appendix A. These results are compared with the simulations of the network system [Eqs. (3)] with the equivalent topological structure. Similarly to what was shown in the globally coupled framework, we perform two different numerical experiments. In the first one, we keep the coupling strength parameter σ fixed and vary the noise intensity level for two different excitability threshold values (i.e., $a = 1.05$ and $a = 1.3$). In the second experiment, we keep the noise intensity fixed and vary the coupling strength σ . The first set of experiments shows the relation between the mean-field approximation and the small noise requirement of the approximation. In the second set of experiments, we see the effect of the distance of the excitable system from the equilibrium point on the mean-field approximation.

The dependence on the noise intensity of the normalized standard deviation R of the ISIs is shown in Fig. 6 for $a = 1.05$ and $a = 1.3$. While the parameters $\varepsilon = 0.01$, $\sigma = 0.1$ have been kept fixed, the noise intensity level D has been varied over logarithmically sampled values between 0.0001 and 10 for both values of a , on the left panel. It can be seen that R depends nonmonotonically on D and a minimum of this quantity is observable for small noise intensity, thus indicating coherence resonance. We remark that in the case of $a = 1.05$, for the mean-field system, the coherence of oscillations grows (R decreases) as we increase the noise intensity D toward the value 6.30957×10^{-4} , where it reaches its highest level, as shown in Fig. 6(a) in terms of dark red downward triangles.

Then it starts decaying as we increase D further. The coherence indicator R shows, for the network system, a pattern similar to the one obtained in the mean-field framework until the noise values are close to and smaller than 10^{-3} , as shown in Fig. 6 in terms of light red diamonds. As we increase the noise intensity D toward values higher than 6.30957×10^{-4} , the coherence of the oscillations starts decreasing and the mean-field curve does not overlap with the one obtained from the network equations any longer. This is due to the fact that we approximate the state variables u and v via Gaussian random processes for small noise intensity values to derive the mean-field system and this approximation does not hold for high noise intensity values (i.e., $D > 6.30957 \times 10^{-4}$). On the right panel, we keep the level of noise intensity fixed and vary the coupling strength. We observe that the mean-field model overlaps with the network in the coherence resonance region, while there is no overlap outside that region.

In the case of $a = 1.3$, the excitable system is further away from the border between excitable and oscillatory regimes in comparison to the case of $a = 1.05$. This results in a rather incoherent spiking of neurons and the Gaussian approximation is not valid, thus affecting the mean-field predictions, as can be seen in Fig. 6(a). On the right panel, where the coupling strength is varied while keeping the noise intensity level fixed, we observe that the mean-field model and the network coincides for high coupling strength values only. In the rest, although they follow the same pattern (almost constant) for small coupling strength values, they do not overlap.

To assess the quality of our assumption about Gaussian distributed variables, we compare the values of the activator variables u_i at each time step with the surrogate values obtained from a Gaussian distribution characterized, at each time, by the same mean and variance. We calculate the Pearson correlation coefficient (PCC) for all times and take the median of the resulting data set. Fig. 7(a) shows the median of the PCC for all noise values, when $a = 1.05$. For low noise values, we stay sufficiently close to 1 for most of the times, indicating a good justification for the Gaussian

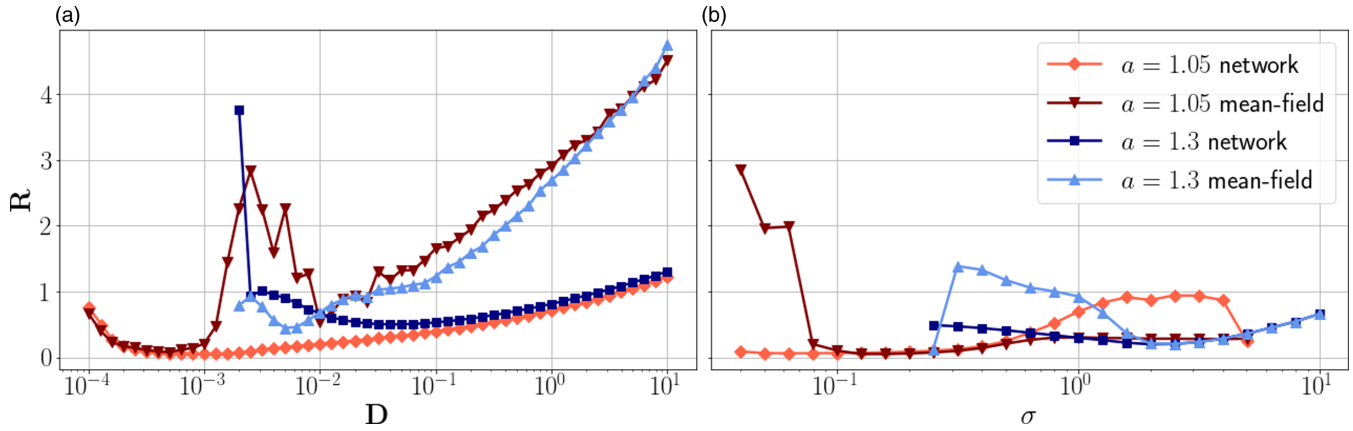


FIG. 6. Normalized standard deviations of the interspike interval R for a locally coupled network and the mean-field system: (a) for fixed coupling strength $\sigma = 0.1$ and varying noise intensity D ; (b) for fixed noise intensity ($D = 0.0005$ for $a = 1.05$ and $D = 0.051$ for $a = 1.3$) and varying coupling strength σ . In both panels, light red diamonds identify the network while dark red downward triangles identify the mean-field results for $a = 1.05$; dark blue squares identify the network while light blue upward triangles identify the mean-field simulations for $a = 1.3$. The results are obtained by integrating over 10 000 time units and then averaging over time, oscillators, and realizations (for five simulations each). The x axis has logarithmic scaling. Other parameters: $N = 100$, $\varepsilon = 0.01$, $\Delta t = 0.001$, $T = M\Delta t = 10\,000$.

assumption. As we are getting closer to 10^{-3} , however, the median decreases significantly, which corroborates our claim that, for higher noise values, the assumption breaks down and with it, the mean-field framework. Further, we demonstrate that, for higher noise values, the distribution of the units is never well approximated with a Gaussian. Comparing the quantile-quantile plots for the cases $D = 0.00063$ Fig. 7(b) and $D = 1.000$ [Fig. 7(c), it clearly results that only the lower noise value approaches the Gaussian assumption sufficiently. The red line indicates a perfect correlation. The quantile-

quantile plots are calculated at the times when PCC reaches its maximum value.

To summarize, in both cases $a = 1.05$ and $a = 1.3$, the mean-field is able to reproduce R patterns, close to the ones of the network, only when the network spikes coherently and the Gaussian assumption about the variables distribution is valid. This happens in a smaller region of the parameter set in comparison to the globally coupled case. In this regime, the variance is low and it is possible to observe a regular spike activity in the mean-field system. For small coupling strength

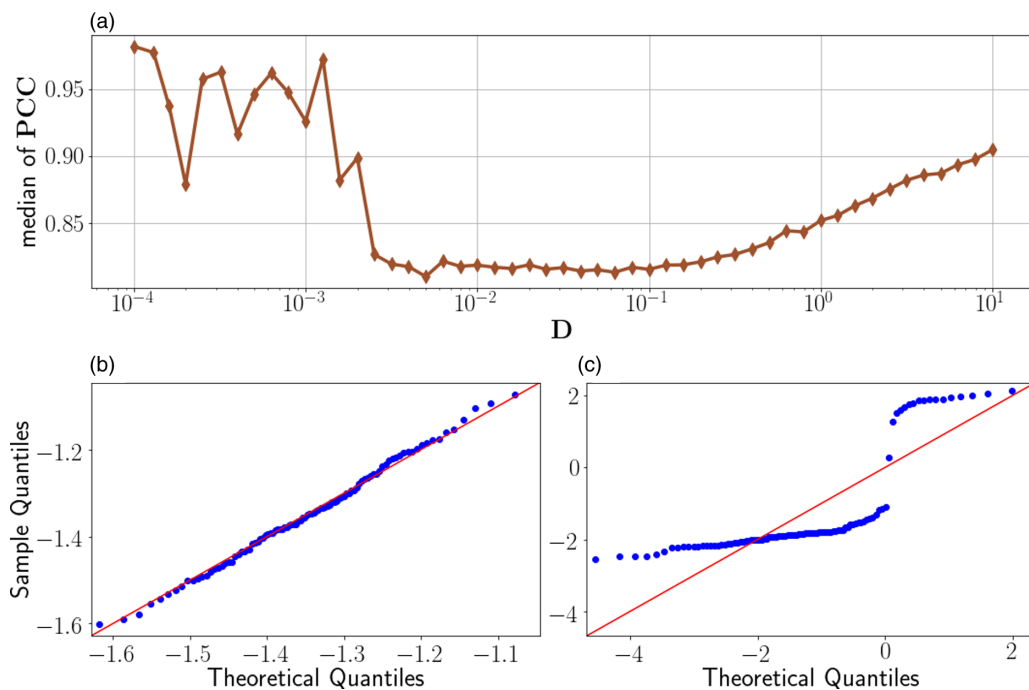


FIG. 7. (a) The median of the PCC for varying noise intensity D . Higher values indicate a better justification for the Gaussian assumption. (b) Quantile-quantile-plot for the best match between a Gaussian distribution and the actual values for $D = 0.00063$ and (c) $D = 1.00$. Other parameters: $a = 1.05$, $\sigma = 0.1$, $N = 100$, $\varepsilon = 0.01$, $\Delta t = 0.001$, $T = M\Delta t = 10\,000$.

values, while there are always some neurons in the network which spike occasionally, it is not possible to observe spike emissions in the mean-field system due to the high variance values at each time instant: due to the high variance, the mean-field system drags u to negative values as soon as u exceeds 0, thus impeding the spike emission. This is at the origin of the different behaviors observable at $a = 1.05$ for small coupling strength values [see Fig. 6(b)]. At $a = 1.3$, the network is further away from the equilibrium point, therefore less neurons spike at small coupling strength values, with respect to the previous case. It results in lower variance values that explain the better agreement with the mean-field system Eqs. (18), since a comparable amount of spikes can be registered in both systems [see Fig. 6(b)]. In Appendix C, we compare the dynamics of a single FHN unit to the dynamics emergent in the locally coupled network for both a cases. It turns out that the mean-field model approximates well the network for low noise intensities, while higher noise intensities cause the network to have similar statistical characteristics as a single unit.

V. CONCLUSION

In this paper, we have developed a mean-field framework that allows analytical treatment of coherence resonance in complex networks of FHNs. In particular, we have compared the obtained results with the direct numerical simulation of the network equations for the locally and globally coupled networks.

For the globally coupled case, we demonstrate good agreement. Moreover, all the nuances of coherence resonance, such as sensitivity to excitability threshold and the coupling strength, are captured by the mean-field framework. On the other hand, for the locally coupled case, we have disagreement for intermediate to large noise values, due to the fact that we approximate the state variables via Gaussian random processes for small noise intensity values. Moreover, in the case of $a = 1.3$, the system is further away from the transition between the excitable and oscillatory regimes compared to the $a = 1.05$ case, thus resulting in rather incoherent spiking. When the system is further from the border between the excitable and oscillatory regimes, the mean-field framework is less effective in reproducing the network dynamics, while, in general, in the locally coupled case, it works well only for small noise values.

The better agreement for the globally coupled case compared to the locally coupled case can be explained by the fact that the two mean-field models are different for the two cases. The locally coupled case needs the variances ρ^2 of u at each time step. Since the excitation travels through the network (compare Fig. 6), the variances become quite large when spikes occur, making it harder, if not impossible, to capture the full dynamics in a mean-field model. The globally coupled case simply takes the mean of all oscillators. As all oscillators have the same coupling term, they also show the same spiking behavior. This high similarity in the behavior leads to a very small variance in u (and v), meaning that the mean-field captures the entire behavior. Further, the better agreement for the globally coupled case compared to the local topology can be explained by the push-pull effect generated

by the all-to-all interaction among the neurons. This allows neurons to spike coherently, while in the locally coupled architecture, due to the absence of such push-pull effect, highly varied spiking patterns emerge for each neuron in the network. This affects the mean-field model via the ρ term, thus preventing the mean-field from giving reasonable insights in the network dynamics [see Eqs. (18)]. More importantly, the system in the locally coupled topology cannot be described in terms of a mean-field framework for higher noise intensities, since the noise dominates the dynamics and the coupling does not come into play. For high noise intensity, the good agreement between the dynamics of a single FHN unit and the locally coupled network shown in Appendix C proves that the neurons behave independently, guided by the noise. This definitively explains the lack of effectiveness of the mean-field model for intermediate to large noise values.

Finally, in the globally coupled system we have found, for the extended model Eqs. (9), anticoherence resonance, which takes place for high noise intensity values. For the extended model, anticoherence is originated from noise-induced activation processes: the noise is so strong that guides neurons over the threshold continuously, thus inducing firing emissions at infinitely small t_{ISI} values. On the contrary, for the original mean-field model Eqs. (8), the anticoherence phenomenon cannot be observed—neither at low nor high intensity values.

Interesting future research directions on the topic would be to extend the mean-field framework to a multilayer topology, where the emergence and control of coherence resonance have been recently found [54,115] and to introduce additional biological features in the model, like chemical synapses, that play functional roles in information processing, similarly to what was shown in Ref. [116] for self-induced stochastic resonance.

ACKNOWLEDGMENTS

This work was supported by the Deutscher Akademischer Austauschdienst (DAAD, German Academic Exchange Service), Project No. 57445304, PPP Frankreich Phase I, and the Deutsche Forschungsgemeinschaft (DFG, German Research Foundation), Project No. 163436311-SFB 910. From the French side, this work was supported by Campus France program PHC PROCOPE 2019, Project No. 42511TA.

APPENDIX A: INTEGRATION SCHEME

In the globally coupled framework, we simulate the system given by Eqs. (9) by employing the classical Euler-Maruyama numerical scheme. The discretized equations read as

$$\begin{aligned} \hat{u}(t_{k+1}) - \hat{u}(t_k) &= \frac{\Delta t}{\varepsilon} \{f(\hat{u}, \hat{v}) + \sigma(\mathbb{E}[\hat{u}(t_k)] - \hat{u}(t_k))\} \\ &\quad + \sqrt{\frac{2\bar{D}}{\varepsilon}} d\hat{W}, \\ \hat{v}(t_{k+1}) - \hat{v}(t_k) &= (\hat{u}(t_k) + a)\Delta t + \sqrt{2\bar{D}} d\hat{W}(t_k), \end{aligned} \quad (\text{A1})$$

where the $\hat{\cdot}$ denotes the discretized variables in time, Δt is the time step, and t_k is the k th sample of time. More precisely, $t_k = k\Delta t$ with $k = 0, 1, \dots, M$, where the initial and final

time instants of the evolution are $t_0 = 0$ and $t_M = T = M\Delta t$, respectively.

In the Euler-Maruyama scheme, the noise terms are discretized as

$$d\tilde{W}(t_k) = \sqrt{\Delta t} \tilde{\mu}(t_k), \quad d\hat{W}(t_k) = \sqrt{\Delta t} \mu(t_k), \quad (\text{A2})$$

where $\tilde{\mu}(t_k)$ and $\mu(t_k)$ are random numbers generated independently from the standard normal distribution at each time instant t_k .

In the locally coupled framework, we simulate the system given by Eqs. (18). We employ the classical Euler-Maruyama numerical scheme where we use the following explicit discretized equations:

$$\begin{aligned} \hat{u}(t_{k+1}) - \hat{u}(t_k) &= \frac{\Delta t}{\varepsilon} \left\{ (1 - \hat{\rho}^2(t_k))\hat{u}(t_k) - \frac{\hat{u}^3(t_k)}{3} - \hat{v}(t_k) \right\}, \\ \hat{v}(t_{k+1}) - \hat{v}(t_k) &= (\hat{u}(t_k) + a)\Delta t + \sqrt{2D}d\hat{W}(t_k), \end{aligned} \quad (\text{A3})$$

where the notation and the parameters are the same as in Eqs. (A1). To perform the numerical integration, the value of $\mathbb{E}[\hat{u}]$ (respectively, $\hat{\rho}^2$) is needed at each time instant t_k for the globally (locally) coupled setting. We find the values of $\mathbb{E}[\hat{u}]$ (respectively, $\hat{\rho}^2$), at each time step, by integrating the network Eqs. (3), with initial conditions generated from a Gaussian distribution and by implementing the Euler-Maruyama method. In particular, we have performed $L = 5$ simulations of globally (locally) coupled networks, where the initial conditions are randomly generated in each simulation. This provides L different sets of $\mathbb{E}[\hat{u}]$ (respectively, $\hat{\rho}^2$) values for each time instant. Finally, the $\mathbb{E}[\hat{u}]$ (respectively, $\hat{\rho}^2$) values to be introduced in the associated mean-field framework, given by Eqs. (A1) [Eqs. (A3)], are determined as the average over L of the values calculated for each time instant.

Finally, we investigate the influence of the time-step size used for the integration of the globally coupled mean-field Eqs. (9). It is important to use a small time step ($\Delta t = 0.001$)

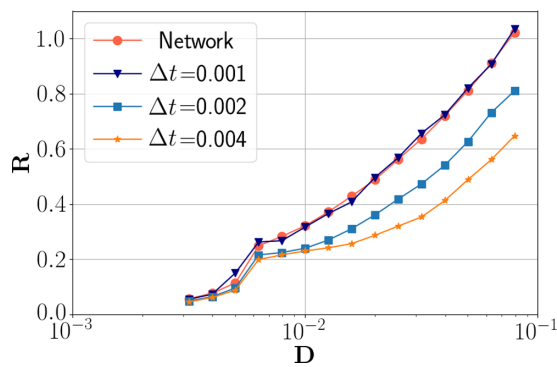


FIG. 8. Normalized standard deviation of the interspike interval R for a globally coupled network ($N = 100$ nodes) and with noise terms in both state variable equations and the same of the corresponding mean-field system simulated with different time steps: $\Delta t = 0.001$ (dark blue triangles), $\Delta t = 0.002$ (light blue squares), and $\Delta t = 0.004$ (orange stars) for fixed coupling strength $\sigma = 0.1$ and varying noise intensity D . The results are obtained by integrating over 5000 time units and then averaging over time and oscillators. The x axis has logarithmic scaling. Other parameters: $a = 1.05$, $\varepsilon = 0.01$.

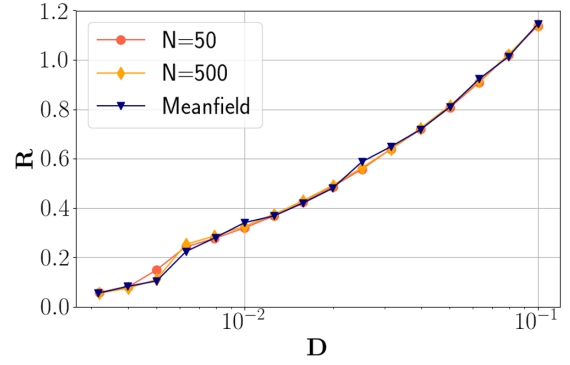


FIG. 9. Normalized standard deviations of the interspike interval R for a globally coupled network (red circles) with noise terms in both system variable equations. Cases with $N = 50$ (red circles) and $N = 500$ nodes (orange diamonds) are compared to the mean-field system (blue triangles) where coupling strength σ is fixed to 0.1 and noise intensity D is varied. The results are obtained by integrating over 5000 time units and then averaging over time and oscillators. The x axis has logarithmic scaling. Other parameters: $a = 1.05$, $\varepsilon = 0.01$.

to achieve good agreement of mean-field results with those obtained from numerical simulation of the network equations (see Fig. 8). Using a larger time step leads to the disagreement of the results for strong noise.

APPENDIX B: DEPENDENCE ON THE NETWORK SIZE

Here we analyze the impact of network size on our results. In more detail, we compare $R(D)$ curves obtained for the globally coupled case from the direct numerical simulation of the network equations for $N = 50$ and $N = 500$ with the curve resulting from the mean-field framework. In particular, for the mean-field model we simulate the system given by Eqs. (9) and, analogously, for the network equations, we integrate Eqs. (3) with noise terms in both system variable equations.

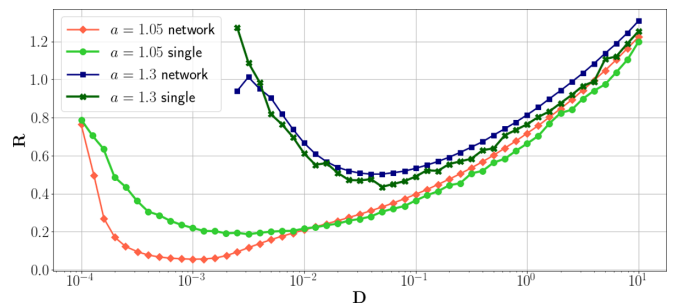


FIG. 10. Comparison between the dynamics emergent in a locally coupled network with the dynamics of a single FHN unit for varying noise intensities D . Both the lower $a = 1.05$ and higher $a = 1.3$ threshold values are shown. The lower value results in an enhanced coherence in the network (red diamonds) compared to the single unit (light green circles), whereas for higher noise intensities the noise dominates the dynamics, which results in a good match. Other parameters: $N = 100$, $\sigma = 0.1$, $\varepsilon = 0.01$, $\Delta t = 0.001$, $T = M\Delta t = 10000$.

It turns out that the system size does not have impact here and all three curves agree well (see Fig. 9).

APPENDIX C: COMPARISON TO THE SINGLE UNIT DYNAMICS

Here we compare the dynamics emergent in a locally coupled network to the one of a single FHN unit. As can be seen in Fig. 10, the R value deviates significantly for low noise intensities. Moreover, the minimum is much more pronounced for

the network case due to the interplay between the individual random processes and the coupling in the network. The probability of a single neuron crossing the threshold is related to the network size, thus, if a single neuron is disturbed enough, it will eventually cause a spike chain over the locally coupled network which ultimately results in a higher coherency. For higher noise intensities, however, the noise dominates the dynamics and therefore the coupling does not come into play. This explains the good agreement between the single unit and the network.

-
- [1] R. L. Stratonovich, *Topics in the Theory of Random Noise* (Gordon and Breach, 1965, 1967), Vols. I and II.
- [2] L. Arnold, *Probability Towards 2000* (Springer, New York, 1998), pp. 34–46.
- [3] V. S. Anishchenko, V. Astakhov, A. B. Neiman, T. Vadivasova, and L. Schimansky-Geier, *Nonlinear Dynamics of Chaotic and Stochastic Systems: Tutorial and Modern Developments* (Springer, Berlin, 2007).
- [4] G. Deco, E. T. Rolls, and R. Romo, *Prog. Neurobiol.* **88**, 1 (2009).
- [5] A. N. Pisarchik, R. Jaimes-Reátegui, C. A. Magallón-García, and C. O. Castillo-Morales, *Biol. Cybern.* **108**, 397 (2014).
- [6] A. E. Runnova, A. E. Hramov, V. V. Grubov, A. A. Koronovskii, M. K. Kurovskaya, and A. N. Pisarchik, *Chaos, Solitons Fractals* **93**, 201 (2016).
- [7] A. Zakharova, T. Vadivasova, V. Anishchenko, A. Koseska, and J. Kurths, *Phys. Rev. E* **81**, 011106 (2010).
- [8] A. Zakharova, J. Kurths, T. Vadivasova, and A. Koseska, *PIOS One* **6** (2011).
- [9] V. S. Anishchenko and A. B. Neiman, *Stochastic Dynamics* (Springer, Heidelberg, 1997), pp. 154–166.
- [10] A. Zakharova, A. Feoktistov, T. Vadivasova, and E. Schöll, *Eur. Phys. J.: Spec. Top.* **222**, 2481 (2013).
- [11] N. Semenova, A. Zakharova, V. S. Anishchenko, and E. Schöll, *Phys. Rev. Lett.* **117**, 014102 (2016).
- [12] A. Zakharova, N. Semenova, V. S. Anishchenko, and E. Schöll, in *Patterns of Dynamics*, edited by P. Gurevich, J. Hell, and B. Sandstede, Springer Proceedings in Mathematics & Statistics Vol 205 (Springer, Berlin, 2017), Vol. 205, p. 44.
- [13] A. Zakharova, N. Semenova, V. S. Anishchenko, and E. Schöll, *Chaos* **27**, 114320 (2017).
- [14] S. Olmi and A. Torcini, in *Nonlinear Dynamics in Computational Neuroscience*, edited by F. Corinto and T. Alessandro, PoliTO Springer Series (Springer International Publishing, Cham, 2019), pp. 65–79.
- [15] A. Zakharova, *Chimera Patterns in Networks: Interplay between Dynamics, Structure, Noise, and Delay*, Understanding Complex Systems (Springer, Cham, 2020).
- [16] R. Benzi, G. Parisi, A. Sutera, and A. Vulpiani, *Tellus* **34**, 10 (1982).
- [17] J. K. Douglass, L. Wilkens, E. Pantazelou, and F. Moss, *Nature* **365**, 337 (1993).
- [18] F. Moss, D. Pierson, and D. O’gorman, *Int. J. Bifurcation Chaos* **4**, 1383 (1994).
- [19] K. Wiesenfeld and F. Moss, *Nature* **373**, 33 (1995).
- [20] Z. Gingl, L. Kiss, and F. Moss, *Europhys. Lett.* **29**, 191 (1995).
- [21] W.-J. Rappel and A. Karma, *Phys. Rev. Lett.* **77**, 3256 (1996).
- [22] A. R. Bulsara and A. Zador, *Phys. Rev. E* **54**, R2185(R) (1996).
- [23] J. J. Collins, T. T. Imhoff, and P. Grigg, *J. Neurophysiol.* **76**, 642 (1996).
- [24] L. Gammaitoni, P. Hänggi, P. Jung, and F. Marchesoni, *Rev. Mod. Phys.* **70**, 223 (1998).
- [25] V. S. Anishchenko, A. B. Neiman, F. Moss, and L. Schimansky-Geier, *Phys. Usp.* **42**, 7 (1999).
- [26] C. B. Muratov, E. Vanden-Eijnden, and E. Weinan, *Physica D* **210**, 227 (2005).
- [27] M. D. McDonnell and D. Abbott, *PLOS Comput. Biol.* **5**, e1000348 (2009).
- [28] L. Gammaitoni, P. Hänggi, P. Jung, and F. Marchesoni, *Eur. Phys. J. B* **69**, 1 (2009).
- [29] V. Semenov, A. Zakharova, Y. Maistrenko, and E. Schöll, *Europhys. Lett.* **115**, 10005 (2016).
- [30] Hu Gang, T. Ditzinger, C. Z. Ning, and H. Haken, *Phys. Rev. Lett.* **71**, 807 (1993).
- [31] A. S. Pikovsky and J. Kurths, *Phys. Rev. Lett.* **78**, 775 (1997).
- [32] A. Neiman, P. I. Saporin, and L. Stone, *Phys. Rev. E* **56**, 270 (1997).
- [33] S.-G. Lee, A. Neiman, and S. Kim, *Phys. Rev. E* **57**, 3292 (1998).
- [34] J. R. Pradines, G. V. Osipov, and J. J. Collins, *Phys. Rev. E* **60**, 6407 (1999).
- [35] G. Giacomelli, M. Giudici, S. Balle, and J. R. Tredicce, *Phys. Rev. Lett.* **84**, 3298 (2000).
- [36] K. Miyakawa and H. Isikawa, *Phys. Rev. E* **66**, 046204 (2002).
- [37] T. Tateno and K. Pakdaman, *Chaos* **14**, 511 (2004).
- [38] B. Lindner, J. Garcia-Ojalvo, A. Neiman, and L. Schimansky-Geier, *Phys. Rep.* **392**, 321 (2004).
- [39] R. E. Lee DeVilleville, E. Vanden-Eijnden, and C. B. Muratov, *Phys. Rev. E* **72**, 031105 (2005).
- [40] O. V. Ushakov, H.-J. Wünsche, F. Henneberger, I. A. Khovanov, L. Schimansky-Geier, and M. Zaks, *Phys. Rev. Lett.* **95**, 123903 (2005).
- [41] P. M. Geffert, A. Zakharova, A. Vüllings, W. Just, and E. Schöll, *Eur. Phys. J. B* **87**, 291 (2014).
- [42] V. Semenov, A. Feoktistov, T. Vadivasova, E. Schöll, and A. Zakharova, *Chaos* **25**, 033111 (2015).
- [43] W. Just, P. M. Geffert, A. Zakharova, and E. Schöll, *Control of Self-Organizing Nonlinear Systems* (Springer International Publishing, Switzerland, 2016), pp. 147–168.

- [44] B. Hu and C. Zhou, *Phys. Rev. E* **61**, R1001(R) (2000).
- [45] A. G. Balanov, N. B. Janson, and E. Schöll, *Physica D* **199**, 1 (2004).
- [46] E. Schöll, A. G. Balanov, N. B. Janson, and A. B. Neiman, *Stoch. Dyn.* **5**, 281 (2005).
- [47] B. Hauschildt, N. B. Janson, A. G. Balanov, and E. Schöll, *Phys. Rev. E* **74**, 051906 (2006).
- [48] D. Ziemann, R. Aust, B. Lingnau, E. Schöll, and K. Lüdge, *Europhys. Lett.* **103**, 14002 (2013).
- [49] P. Balenzuela, P. Rué, S. Boccaletti, and J. García-Ojalvo, *New J. Phys.* **16**, 013036 (2014).
- [50] M. Masoliver, N. Malik, E. Schöll, and A. Zakharova, *Chaos* **27**, 101102 (2017).
- [51] R. Aust, P. Hövel, J. Hizanidis, and E. Schöll, *Eur. Phys. J.: Spec. Top.* **187**, 77 (2010).
- [52] T. Kreuz, S. Luccioli, and A. Torcini, *Phys. Rev. Lett.* **97**, 238101 (2006).
- [53] T. Kreuz, S. Luccioli, and A. Torcini, *Neurocomputing* **70**, 1970 (2007).
- [54] N. Semenova and A. Zakharova, *Chaos* **28**, 051104 (2018).
- [55] Y. Wang, D. T. W. Chik, and Z. D. Wang, *Phys. Rev. E* **61**, 740 (2000).
- [56] O. Kwon and H. T. Moon, *Phys. Lett. A* **298**, 319 (2002).
- [57] X. Sun, Q. Lu, and J. Kurths, *Physica A* **387**, 6679 (2008).
- [58] E. Yilmaz, M. Ozer, V. Baysal, and M. Perc, *Sci. Rep.* **6**, 30914 (2016).
- [59] A. V. Andreev, V. V. Makarov, A. E. Runnova, A. N. Pisarchik, and A. E. Hramov, *Chaos, Solitons Fractals* **106**, 80 (2018).
- [60] N. Brunel and X.-J. Wang, *J. Neurophysiol.* **90**, 415 (2003).
- [61] G. Deco and M. L. Kringelbach, *Trends Neurosci.* **39**, 125 (2016).
- [62] A. Pisarchik, V. A. Maksimenko, A. V. Andreev, N. S. Frolov, V. V. Makarov, M. O. Zhuravlev, A. E. Runnova, and A. E. Hramov, *Sci. Rep.* **9**, 18325 (2019).
- [63] C. Kirst, M. Timme, and D. Battaglia, *Nat. Commun.* **7**, 1 (2016).
- [64] A. Palmigiano, T. Geisel, F. Wolf, and D. Battaglia, *Nat. Neurosci.* **20**, 1014 (2017).
- [65] B. van Wijk, P. J. Beek, and A. Daffertshofer, *Front. Hum. Neurosci.* **6**, 252 (2012).
- [66] B. Horwitz and A. R. Braun, *Brain and language* **89**, 377 (2004).
- [67] D. H. Hubel and T. N. Wiesel, *J. Physiol. (Lond.)* **148**, 574 (1959).
- [68] D. H. Hubel and T. N. Wiesel, *J. Physiol. (Lond.)* **160**, 106 (1962).
- [69] B. B. Averbeck, P. E. Latham, and A. Pouget, *Nat. Rev. Neurosci.* **7**, 358 (2006).
- [70] G. Citti and A. Sarti, *J. Math. Imaging Vision* **24**, 307 (2006).
- [71] A. Sarti, G. Citti, and J. Petitot, *Biol. Cybern.* **98**, 33 (2008).
- [72] E. Baspinar, G. Citti, and A. Sarti, *J. Math. Imaging Vision* **60**, 900 (2018).
- [73] E. Baspinar, A. Sarti, and G. Citti, *J. Math. Neurosci.* **10**, 1 (2020).
- [74] R. Toral, C. R. Mirasso, and J. D. Gunton, *Europhys. Lett.* **61**, 162 (2003).
- [75] W. Du-Qu and L. Xiao-Shu, *Commun. Theor. Phys.* **48**, 759 (2008).
- [76] B. Lindner and L. Schimansky-Geier, *Phys. Rev. E* **60**, 7270 (1999).
- [77] S. Olmi, D. Angulo-Garcia, A. Imparato, and A. Torcini, *Sci. Rep.* **7**, 1 (2017).
- [78] D. M. Abrams, and S. H. Strogatz, *Phys. Rev. Lett.* **93**, 174102 (2004).
- [79] J. Baladron, D. Fasoli, O. Faugeras, and J. Touboul, *J. Math. Neurosci.* **2**, 10 (2012).
- [80] M. Bossy, O. Faugeras, and D. Talay, *J. Math. Neurosci.* **5**, 19 (2015).
- [81] J. A. White, J. T. Rubinstein, and R. Alan, *Trends Neurosci.* **23**, 131 (2000).
- [82] W. H. Calvin and C. F. Stevens, *Science* **155**, 842 (1967).
- [83] M. E. Yamakou, T. D. Tran, L. H. Duc, and J. Jost, *J. Math. Biol.* **79**, 509 (2019).
- [84] N. Berglund and G. Barbara, *Noise-Induced Phenomena in Slow-Fast Dynamical Systems: A Sample-Paths Approach* (Springer Science & Business Media, London, UK, 2006).
- [85] N. Berglund, B. Gentz, and C. Kuehn, *J. Diff. Equ.* **252**, 4786 (2012).
- [86] A. L. Hodgkin and A. F. Huxley, *J. Physiol. (Lond.)* **117**, 500 (1952).
- [87] C. Morris and H. Lecar, *Biophys. J.* **35**, 193 (1981).
- [88] J. L. Hindmarsh and R. Rose, *Proc. R. Soc. London B* **221**, 87 (1984).
- [89] W. Gerstner and W. M. Kistler, *Spiking Neuron Models: Single Neurons, Populations, Plasticity* (Cambridge University Press, Cambridge, UK, 2002).
- [90] R. Brette, M. Rudolph, T. Carnevale, M. Hines, D. Beeman, J. M. Bower, M. Diesmann, A. Morrison, P. H. Goodman, F. C. Harris *et al.*, *J. Comput. Neurosci.* **23**, 349 (2007).
- [91] E. M. Izhikevich, *Dynamical Systems in Neuroscience* (MIT Press, Cambridge, Massachusetts, US 2007).
- [92] A. Galves and E. Löcherbach, *J. Stat. Phys.* **151**, 896 (2013).
- [93] H. R. Wilson and J. D. Cowan, *Biophys. J.* **12**, 1 (1972).
- [94] H. R. Wilson and J. D. Cowan, *Kybernetik* **13**, 55 (1973).
- [95] J. Touboul, G. Hermann, and O. Faugeras, *SIAM J. Appl. Dyn. Syst.* **11**, 49 (2012).
- [96] E. Montbrió, D. Pazó, and A. Roxin, *Phys. Rev. X* **5**, 021028 (2015).
- [97] F. Devalle, A. Roxin, and E. Montbrió, *PLoS Comput. Biol.* **13**, e1005881 (2017).
- [98] A. Ceni, S. Olmi, A. Torcini, and D. Angulo-Garcia, *Chaos* **30**, 053121 (2020).
- [99] M. Segneri, H. Bi, S. Olmi, and A. Torcini, *Front. Comput. Neurosci.* **14**, 47 (2020).
- [100] G. B. Ermentrout and N. Kopell, *SIAM J. Appl. Math.* **46**, 233 (1986).
- [101] R. FitzHugh, *Biophys. J.* **1**, 445 (1961).
- [102] J. Nagumo, S. Arimoto, and S. Yoshizawa, *Proc. IRE* **50**, 2061 (1962).
- [103] N. Burić, D. Ranković, K. Todorović, and N. Vasović, *Physica A* **389**, 3956 (2010).
- [104] R. Rodriguez and H. C. Tuckwell, *Phys. Rev. E* **54**, 5585 (1996).
- [105] H. Tuckwell, *J. Comput. Neurosci.* **5**, 91 (1998).
- [106] S. Tanabe and K. Pakdaman, *Phys. Rev. E* **63**, 031911 (2001).
- [107] M. Zaks, X. Sailer, L. Schimansky-Geier, and A. Neiman, *Chaos* **15**, 026117 (2005).
- [108] N. Etemadi, *Z. Wahrscheinlichkeitstheor. Verwandte Geb.* **55**, 119 (1981).

- [109] D. Golomb, D. Hansel, and G. Mato, *Handbook of Biological Physics* (Elsevier, 2001), Vol. 4, pp. 887–968.
- [110] S. Olmi, R. Livi, A. Politi, and A. Torcini, *Phys. Rev. E* **81**, 046119 (2010).
- [111] S. Luccioli, S. Olmi, A. Politi, and A. Torcini, *Phys. Rev. Lett.* **109**, 138103 (2012).
- [112] A. M. Lacasta, F. Sagués, and J. M. Sancho, *Phys. Rev. E* **66**, 045105(R) (2002).
- [113] B. Lindner, L. Schimansky-Geier, and A. Longtin, *Phys. Rev. E* **66**, 031916 (2002).
- [114] S. Luccioli, T. Kreuz, and A. Torcini, *Phys. Rev. E* **73**, 041902 (2006).
- [115] M. E. Yamakou and J. Jost, *Phys. Rev. E* **100**, 022313 (2019).
- [116] M. E. Yamakou, P. G. Hjorth, and E. A. Martens, *Front. Comput. Neurosci.* **14**, 62 (2020).